International Journal of Heat and Mass Transfer 158 (2020) 119997

Contents lists available at ScienceDirect

International Journal of Heat and Mass Transfer

journal homepage: www.elsevier.com/locate/hmt

Impacting-freezing dynamics of a supercooled water droplet on a cold surface: Rebound and adhesion

Xuan Zhang[a], Xin Liu[b], Xiaomin Wu[a,*], Jingchun Min[b,*]

[a] Key Laboratory for Thermal Science and Power Engineering of Ministry of Education, Beijing Key Laboratory for CO_2 Utilization and Reduction Technology, Department of Energy and Power Engineering, Tsinghua University, Beijing 100084, China
[b] Key Laboratory for Thermal Science and Power Engineering of Ministry of Education, Department of Engineering Mechanics, Tsinghua University, Beijing 100084, China

ARTICLE INFO

Article history:
Received 23 March 2020
Revised 18 May 2020
Accepted 25 May 2020
Available online 30 June 2020

Keywords:
Impacting
Freezing
Supercooling
Droplet
Rebound and adhesion

ABSTRACT

The impacting-freezing dynamics of a supercooled water droplet on a cold surface is studied experimentally and numerically. A numerical model that considers both the effects of the supercooling degree on the physical properties and of the dynamic contact angle on the contact line motion is established to simulate the droplet impacting-freezing behaviors using the VOF multiphase model and the Solidification/Melting phase change model. Experiments are also conducted for the impacting-freezing processes of supercooled and room temperature water droplets on a cold surface and for the impacting process of a room temperature droplet on a room temperature surface. Both the temporal droplet profile and the spreading factor calculated by the simulations agree well with the experimental observations. The maximum deviation of the maximum and stable spreading factors between experiments and simulations is 11.3%. The numerical and experimental results elucidate that the supercooled droplet spreads and retracts slower than the room temperature one in the impacting process and thus yields a smaller maximum and a larger stable spreading factor. The increases of the Weber number and supercooling degree and the decrease of the contact angle will enlarge the above differences. Additionally, three different morphologies of full rebound, partial rebound and full adhesion are identified in the impacting-freezing process of a supercooled droplet on a cold hydrophobic surface, indicating the competition between the fluid flow and heat transfer. A unified morphology map of rebound and adhesion correlating the Weber number, supercooling degree and contact angle is proposed for the impacting-freezing behavior and it presents the universal limits for the full rebound and adhesion. This work may deepen our understanding of the interaction mechanism between the droplet and cold surface in the impacting-freezing process and provides reference for the associated applications and technologies in anti-icing/frosting and self-cleaning.

1. Introduction

The impacting-freezing phenomena of a supercooled water droplet on a cold surface widely exist in natural and engineering processes. In aerospace, aircraft icing caused by the impacting and freezing of supercooled water droplets on the wing greatly reduces the lift and increases the drag, constituting a huge threat to the aircraft flight safety [1,2]. Similarly, icing on wind turbines or transmission lines in the power sector may result in various problems [3]. Furthermore, the formations of the hail in meteorology [4] and the frost in refrigeration [5,6] are also closely related to the freezing of supercooled water droplets. Study on the impacting-freezing process of a supercooled water droplet can help to better understand the mechanisms of the ice/frost formation and accumulation, explore and improve the design of anti-icing/frosting surface [7,8], and even provide insights into the 3D printing [9] and other material technologies related to solidification [10].

The impacting-freezing phenomenon of a supercooled water droplet actually involves two processes of impacting and freezing. For each separate individual process, many solid foundation works have been done. As described by previous studies [11,12], the droplet impacting on a solid surface generally experiences the spreading, retraction, oscillation, splash, rebound or adhesion stages. The impacting process could be influenced by the fluid property, impact velocity, droplet size, and surface characteristics [11-14]. Recently, more attention is attracted by the rebound of an impacting droplet [15], especially on the superhydrophobic surface [16], because it directly dominates the surface ice-phobic perfor-

* Corresponding authors.
E-mail addresses: wuxiaomin@mail.tsinghua.edu.cn (X.M. Wu), minjc@mail.tsinghua.edu.cn (J.C. Min).

https://doi.org/10.1016/j.ijheatmasstransfer.2020.119997
0017-9310/

Nomenclature

A_{mush}	mushy zone constant
c	specific heat, J kg^{-1} K^{-1}
Ca	Capillary number
D	diameter, m
f, f^{-1}	function and inverse function
$\boldsymbol{F}_{st}$	volumetric surface tension force, N m^{-3}
$\boldsymbol{g}$	gravity acceleration, m s^{-2}
h	enthalpy, J kg^{-1}
k	thermal conductivity, W m^{-1} K^{-1}
L	latent heat of solidification, J kg^{-1}
$\boldsymbol{n}$	unit normal vector, m
Re	Reynold number
S_E	energy source term, J m^{-3} s^{-1}
$\boldsymbol{S}_M$	momentum source term, N m^{-3}
St	Stefan number
t	time, s
T	temperature, °C
T_a	ambient air temperature, °C
T_s	cold surface temperature, °C
T_F	freezing temperature (point), °C
$T_{Liquidus}$	liquidus temperature, °C
$T_{Solidus}$	solidus temperature, °C
ΔT_{SC}	supercooling degree, $T_F - T_0$, °C
ΔT_F	phase change temperature range, $T_{Liquidus} - T_{Solidus}$, °C
$\boldsymbol{u}$	velocity vector, m s^{-1}
U	velocity, m s^{-1}
V	volume, m^3
We	Weber number
X	physical properties

Greek symbols

α_1, α_2	volume fractions of the primary (air) and secondary (water-ice) phases
α_{Liquid}	liquid water fraction in the secondary (water-ice) phase
β	mass fraction
θ	contact angle, °
θ_{adv}	advancing contact angle, °
θ_d	dynamic contact angle, °
θ_{eq}	equilibrium contact angle, °
θ_{rec}	receding contact angle, °
θ_{sta}	static contact angle, °
κ	curvature, m^{-1}
μ	viscosity, Pa s
ρ	density, kg m^{-3}
σ	surface tension, N m^{-1}
$\boldsymbol{\tau}$	unit tangential vector, m

Subscripts

0	initial
i	ice
m	mixture
max	maximum
p	pth phase, $p = 1, 2$
s	surface
w	water
F	freezing
CL	contact line
RT	room temperature
SC	supercooling or supercooled
ST	surface tension
Ref	reference
DCA	dynamic contact angle

mance. The freezing process of a sessile supercooled water droplet on a cold surface can be divided into five distinct stages based on its temperature transition characteristics [17-19], including: (1) liquid cooling (supercooling), (2) nucleation, (3) recalescence, (4) solidification, and (5) solid cooling. The nucleation is the starting point of the recalescence and may occur spontaneously. Due to its randomness, the nucleation is related to the droplet volume [20], surface characteristics [21] and pressure [22], especially affected by shock vibration [23]. During the subsequent recalescence stage, the supercooling drives rapid kinetic crystal growths from crystal nuclei inside the droplet. The droplet changes into a uniform water-ice mixture, with its temperature reverting to the freezing point (0 °C) due to the latent heat release and its volume expanding because of the density sudden change [24,25]. Then, the freezing front advances from the droplet bottom to the top side until the remaining water-ice mixture is completely solidified and a conical tip finally forms [26,27]. The final freezing time could be controlled by the droplet volume, surface temperature and its wettability [28,29].

Compared with the separate researches on the above two aspects, investigations on the mechanisms of impacting-freezing process of a supercooled water droplet on the cold surface are facing more challenges and difficulties mainly caused by the metastable supercooled water. More studies focused on the impacting-freezing process of a room temperature droplet on the cold surface. Mishchenko et al. [30] designed ice-free nanostructured surfaces based on repulsion of impacting water droplets. Their experimental analysis showed that highly ordered superhydrophobic materials could keep the surface entirely ice-free down to −25 °C ~ −30 °C because the droplet was removed before ice nucleation occurred. Jin et al. [31-33] experimentally investigated the impacting-freezing process of a water droplet on cold spherical and cylindrical surfaces, they also reported the observations of the successive freezing processes of water droplets on an ice surface. They found that the spreading factors at low surface temperature cases were larger than that of the room temperature case. Schremb et al. [34] experimentally discovered that the nucleation rate in the impacting drop is not constant from the statistical results. Ding et al. [35] visually studied the dynamic behavior of a water droplet impacting on the superhydrophobic surface with different inclinations and supercooling degrees, they observed that the droplet successively undergoes full rebound, partial rebound and no rebound with the gradually decreasing surface temperature. Chen et al. [36] and Maitra et al. [37] investigated the droplet bouncing on the hierarchical branched nanotube arrays and superhydrophobic surfaces below 0 °C. Yao et al. [38] used the VOF and Solidification/Melting model to simulate the freezing of a room temperature water droplet impacting on the cold surface.

As for the impacting-freezing process of a supercooled water droplet on a cold surface, some experimental and numerical works are also seen in recent years. Zhang et al. [39] experimentally investigated the impacting behaviors between supercooled droplets and various textured superhydrophobic surfaces and concluded that the dramatic increase of the liquid–solid contact area leads to a larger nucleation rate and a lower critical adhesion temperature. Liu et al. [40,41] experimentally measured the impact freezing modes of supercooled droplets determined by both nucleation and icing evolution and found two frozen morphologies of droplets. Blake et al. [42], Yao et al. [43] and Chang et al. [44] simulated the freezing of supercooled water droplets impacting a cooled superhydrophobic substrate using the VOF and Solidification/Melting

model. Tembely et al. [45] further introduced the nucleation theory in the simulation. Schremb et al. [46] experimentally and theoretically studied the interaction between fluid flow and solidification during the impacting of supercooled water drops onto an ice surface. It is shown that the drop temperature has a dominating influence on the lamella thinning and the final ice layer thickness.

Although many works have been done on the droplet impacting and freezing, most of them separately investigated the characteristics of impacting and freezing, or focused on the impacting-freezing process of a room temperature droplet on a cold surface. Recently, the impacting-freezing coupled dynamics of a supercooled droplet on a cold surface begins to attract research attention, but more efforts are still needed to figure out the interaction mechanism between the supercooled droplet and the cold surface. Additionally, previous studies partially concentrated on the motion of the contact line and the nucleation during the impacting-freezing process. The competition between the fluid flow and heat transfer during the impacting-freezing process is rarely reported and this significantly determines the surface's anti-icing/frosting performance. There is an urgent need to establish a unified morphology of rebound and adhesion after a supercooled droplet impacts the cold surface

In this work, we numerically and experimentally study the impacting-freezing characteristics of a supercooled water droplet on a cold surface. A numerical model involving the VOF multiphase model and the Solidification/Melting model in CFD software is built to simulate the droplet impacting and freezing behaviors. After comparing the simulation and experiment results, we investigate the effects of the Weber number, contact angle and supercooling degree on the impacting-freezing process, including the spreading factor and the droplet morphology of rebound and adhesion, to reveal the competition between the impacting and freezing processes of a supercooled droplet on the cold surface.

2. Simulation model

As shown in Fig. 1, when a supercooled water droplet impacts on a cold solid surface, it will conventionally experience spreading, receding, oscillating and stable stages like a room temperature droplet impacting a room temperature surface [11-14]. Due to the existence of the supercooled water and cold surface, the droplet will also undergo the liquid supercooling, nucleation, recalescence, freezing and solid cooling stages [17,18] (Fig. 1). The multiphase fluid flow and heat transfer (phase change) are coupled in the impacting-freezing process of a supercooled water droplet on the cold surface. Since the vibration induced by the impacting process could significantly enhance the nucleation in the freezing process [23,40], the nucleation occurs upon the impacting droplet touching the cold surface, and the recalescence spreads much faster than the contact line. Thus, the supercooled impacting water droplet with an initial velocity of U_0 and an initial temperature of T_0 (Fig. 1a) is assumed to complete the nucleation-recalescence stage upon touching the cold surface or in a very short time (Fig. 1b). The supercooled droplet changes into a water-ice mixture instantaneously, which has different physical properties from the water. Its volume and diameter change from V_0 and D_0 to V_{mix} and D_{mix} (the details will be introduced in Section 2.2) with its temperature T_0 recovering to the freezing point T_F (0 °C) [24,25]. To compare with the impacting dynamics of a room temperature droplet, the droplet impacting parameters here are still defined as $We = \rho U_0^2 D_0/\sigma$ and $Re = \rho U_0 D_0/\mu$. After impacting on the cold surface, the droplet deforms and the contact line spreads under the action of the inertia force, surface tension and gravity, accompanied by the propagation of the freezing front along the cold surface inside the droplet (Fig. 1c) [46,47]. The spreading factor β is defined as the ratio of spreading diameter to initial diameter, that is $\beta = D/D_0$. Then, the droplet starts to recede after reaching the maximum spreading state (Fig. 1d). During the spreading or receding stages, the contact line may be frozen and cannot move anymore. The spreading diameter at this time is the frozen (stable) diameter D_F. The upper part of the droplet continues oscillating with the freezing front advancing from the bottom to the top (Fig. 1e) until the water-ice mixture becomes completely solidified (Fig. 1f). A conical tip forms at the end of the freezing process [18,26,48].

2.1. VOF (Volume of fluid) method and DCA (Dynamic contact angle) model

Owing to existence of the multiphase flow in the droplet impacting-freezing process on a cold surface, the VOF (Volume of

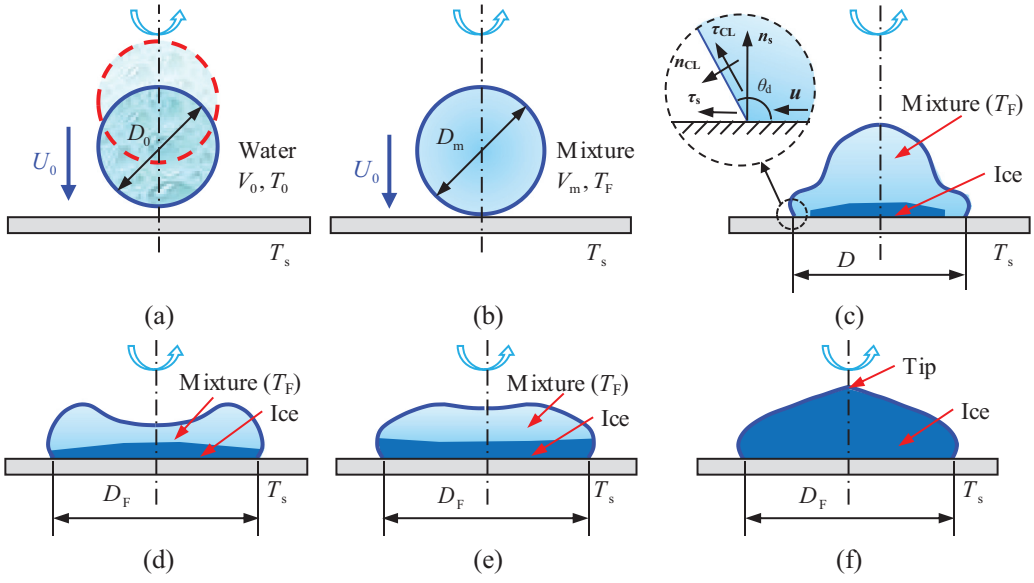

Fig. 1. Schematic of the impacting-freezing process of a supercooled water droplet on a cold surface: (a) before touching the surface (supercooling stage), (b) upon touching the surface (nucleation-recalescence stage), (c) spreading stage (freezing stage), (d) receding stage (freezing stage), (e) oscillating stage (freezing stage), (f) stable stage (completely frozen).

Fluid) method described by Hirt and Nichols [49] is used to capture the mass and momentum transfer of each phase in this study. The tracking of the interface between the phases is accomplished by the solution of a continuity equation for the volume fraction of one (or more) phase [50]. The volume fraction of the pth phase in each cell is defined as

$$\alpha_p = \frac{\text{volume of } p\text{th phase}}{\text{cell volume}} \tag{1}$$

and $\sum \alpha_p = 1$.

In this study, the unfrozen water-ice mixture and frozen ice are taken as one liquid phase in the Solidification/Melting model (to be introduced in the following Section 2.3) applied to dealing with the phase change process. Thus, two phases exist in each cell and the volume fraction of the secondary liquid phase α_2 in each cell can be expressed as

$$\alpha_1 = \begin{cases} 1 & , \quad \text{if the cell is occupied by gas} \\ 0 < \alpha_1 < 1 & , \quad \text{if the cell contains gas and liquid} \\ 0 & , \quad \text{if the cell is occupied by liquid} \end{cases} \tag{2}$$

which satisfies

$$\alpha_1 + \alpha_2 = 1 \tag{3}$$

The mass conservation equations of the liquid and gas phases are expressed by

$$\frac{\partial}{\partial t}(\alpha_p \rho_p) + \nabla \cdot (\alpha_p \rho_p \boldsymbol{u}) = 0 \ , \quad p = 1,\ 2 \tag{4}$$

while a single momentum conservation is shared throughout the computational domain, i.e.,

$$\frac{\partial}{\partial t}(\rho \boldsymbol{u}) + \nabla \cdot (\rho \boldsymbol{u}\boldsymbol{u}) = -\nabla p + \nabla \cdot \mu\left[\nabla \boldsymbol{u} + (\nabla \boldsymbol{u})^{\mathrm{T}}\right] + \rho \boldsymbol{g} + \boldsymbol{F}_{\mathrm{ST}} + \boldsymbol{S}_{\mathrm{M}} \tag{5}$$

in which $\boldsymbol{F}_{\mathrm{ST}}$ is the volumetric surface tension force acting on the fluid at the gas-liquid interface and $\boldsymbol{S}_{\mathrm{M}}$ is the momentum source term which is introduced by the freezing process and obtained by Eq. (24). In the references [51-54], many previous researchers used the continuum surface force (CSF) model proposed by Brackbill et al. [50] to calculate the surface tension force when simulating the droplet impacting process. Considering the good agreements between their simulations and experiments, the CSF model is also adopted in the present work. The model defines $\boldsymbol{F}_{\mathrm{st}}$ by

$$\boldsymbol{F}_{\mathrm{st}} = \sigma \frac{\rho \kappa \ \nabla \alpha_1}{(\rho_1 + \rho_2)/2} \tag{6}$$

where κ is the curvature of the interface. It can be calculated from the divergence of the unit normal vector $\boldsymbol{n}$ of gas-liquid interface, which can be expressed as the gradient of the volume fraction, i.e.,

$$\kappa = \nabla \cdot \boldsymbol{n} \ , \quad \boldsymbol{n} = \frac{\nabla \alpha_1}{|\nabla \alpha_1|} \tag{7}$$

In above Eqs. (4)~(6), the fluid density ρ, viscosity μ and thermal conductivity k are temperature-dependent and defined by

$$\rho = \sum_p \alpha_p \rho_p,\ \mu = \sum_p \alpha_p \mu_p,\ k = \sum_p \alpha_p k_p,\ p = 1, 2 \tag{8}$$

At the solid surface, the body force term $\boldsymbol{F}_{\mathrm{ST}}$ in the momentum equation is considered through the wall adhesion forces acting at the contact line. As shown in Fig. 1c, the wall adhesion is related to the contact angle θ_{d} which is defined as the angle between the solid surface (the opposite direction of $\boldsymbol{\tau}_{\mathrm{s}}$) and the tangential vector $\boldsymbol{\tau}_{\mathrm{CL}}$ of the interface at the contact line.

The unit vector $\boldsymbol{n}_{\mathrm{CL}}$ normal to the liquid-gas interface at the contact line (one cell away from the solid surface in the calculation) is used to adjust the local curvature of the interface near the solid surface, and it can be calculated from the contact angle θ_{d} by

$$\boldsymbol{n}_{\mathrm{CL}} = \left(\frac{\nabla \alpha_1}{|\nabla \alpha_1|}\right)_{\mathrm{CL}} = \boldsymbol{n}_{\mathrm{s}} \cos\theta_{\mathrm{d}} + \boldsymbol{\tau}_{\mathrm{s}} \sin\theta_{\mathrm{d}} \tag{9}$$

where $\boldsymbol{n}_{\mathrm{s}}$ and $\boldsymbol{\tau}_{\mathrm{s}}$ are the unit vectors normal and tangential to the solid surface, respectively. The combination of this contact angle with the calculated surface vectors determines the local curvature of the interface, and it is used to adjust the body force term $\boldsymbol{F}_{\mathrm{ST}}$ at the contact line.

The contact angle θ_{d} is constant for an ideal smooth surface, but it varies with contact line velocity on a real surface because of the contact angle hysteresis induced by the surface roughness, namely the dynamic contact angle [55]. After comparing results yielded by several DCA (Dynamic Contact Angle) models [13,55,56], the empirical model proposed by Kistler is adopted to calculate the dynamic contact angle θ_{d} in the present research. Previous researchers using this model obtained good agreements between the dynamic contact angles yielded by their simulations and experiments [51,52]. In the model, the dynamic contact angle θ_{d} is defined as

$$\theta_{\mathrm{d}} = f_{\mathrm{Hoff}}\left[Ca + f_{\mathrm{Hoff}}^{-1}(\theta_{\mathrm{eq}})\right] \tag{10}$$

in which $f_{\mathrm{Hoff}}(x)$ is the Hoffman function [57], given by

$$f_{\mathrm{Hoff}} = \arccos\left\{1 - 2\tanh\left[5.16\left(\frac{x}{1 + 1.31x^{0.99}}\right)^{0.706}\right]\right\} \tag{11}$$

and $f_{\mathrm{Hoff}}^{-1}(x)$ is its inverse function, while x is the argument of the function. Further, $Ca = \mu U_{\mathrm{CL}}/\sigma$ is the Capillary number, in which U_{CL} is the contact line velocity along the tangential vector of the solid surface, calculated by

$$U_{\mathrm{CL}} = \boldsymbol{u}_{\mathrm{CL}} \cdot \boldsymbol{\tau}_{\mathrm{s}} \tag{12}$$

and θ_{eq} is the equilibrium contact angle and has different values in the advancing and receding processes of the contact line, which can be expressed as

$$\theta_{\mathrm{eq}} = \begin{cases} \theta_{\mathrm{adv}} & , \quad U_{\mathrm{CL}} > 0 \\ \theta_{\mathrm{rec}} & , \quad U_{\mathrm{CL}} < 0 \end{cases} \tag{13}$$

where θ_{adv} and θ_{rec} are the advancing and receding contact angles. Fig. 2 illustrates the relationship between the dynamical angle θ_{d} and the Capillary number Ca (or the contact line velocity U_{CL}) for the surfaces used in our experiments and simulations.

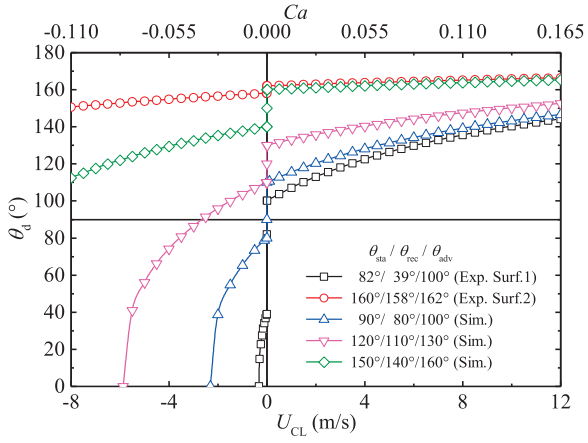

Fig. 2. Relationship between the dynamic contact angle and the Capillary number (or the contact line velocity) for the surfaces used in the present experiments and simulations.

2.2. Consideration of supercooling degree

As indicated in Fig. 1b, the supercooled water droplet will experience the nucleation-recalescence stage and the supercooled water droplet changes into the water-ice mixture [18,25], which will affect the physical properties. The ice mass fraction (β_i) in the mixture can be calculated from the energy balance [18,58] as follows,

$$\beta_i = \frac{c_{w,T_F}(T_F - T_0)}{L} = \frac{c_{w,T_F}\Delta T_{SC}}{L} = \frac{c_{w,T_F}}{c_i}St \tag{14}$$

where $\Delta T_{SC} = T_F - T_0$ denotes the supercooling degree, and St expresses the Stefan number, given by $St = c_i\Delta T/L$, which is the ratio of the sensible to latent heat [59]. So, the latent heat of solidification and the physical properties of the water-ice mixture including the density, specific heat and thermal conductivity at the end of the nucleation/recalescence stage can be calculated from

$$L_m = (1 - \beta_i)L \tag{15}$$

$$\rho_m = \rho_w(1-\beta_i) + \rho_i\beta_i,\ c_m = c_w(1-\beta_i) + c_i\beta_i,\ k_m = k_w(1-\beta_i) + k_i\beta_i \tag{16}$$

As stated in the assumption, the supercooled water droplet completes the nucleation-recalescence stage upon touching the cold surface or in a very short time. The droplet thus remains almost a sphere and its volume and diameter can be obtained from

$$V_m = \frac{\rho_w V_0}{\rho_m},\ D_m = \sqrt[3]{\frac{\rho_w}{\rho_m}}D_0 \tag{17}$$

All parameters calculated from the above Eqs. (15)–(17) serve as the initial conditions for the subsequent impacting-freezing process.

2.3. Solidification/Melting model

With the VOF method capturing the mass and momentum transfer, the Solidification/Melting model is here used to calculate the heat transfer in the impacting-freezing process. The model treats the water-ice mixture (droplet) as one liquid phase whose latent heat and thermophysical properties can be obtained from Eqs. (15) and (16) after the nucleation-recalescence stage. In the phase change process, the liquid fraction in each cell is calculated using the enthalpy-porosity method based on the enthalpy balance [50]. The total enthalpy in each cell, which is filled with liquid and solid, can be computed as the sum of the sensible enthalpy and latent heat, i.e.

$$h = h_{Sensible} + h_{Latent} \tag{18}$$

where the sensible enthalpy is expressed as

$$h_{Sensible} = h_{Ref} + \int_{T_{Ref}}^{T} c\mathrm{d}T \tag{19}$$

in which h_{Ref} and T_{Ref} the reference enthalpy and temperature, and the latent heat is defined as

$$h_{Latent} = \alpha_{Liquid}L_m \tag{20}$$

in which α_{Liquid} is the liquid fraction, given by

$$\alpha_{Liquid} = \begin{cases} 0 & T < T_{Solidus} \\ \frac{T - T_{Solidus}}{T_{Liquidus} - T_{Solidus}} & T_{Solidus} < T < T_{Liquidus} \\ 1 & T > T_{Liquidus} \end{cases} \tag{21}$$

where $T_{Solidus} = T_F - \Delta T_F/2$ and $T_{Liquidus} = T_F + \Delta T_F/2$ are the solidus and liquidus temperatures, and ΔT_F stands for the phase change temperature range, which has a small value and is used to smooth the sharp changes in the temperature-dependent physical properties at the freezing temperature to ensure the convergence of the calculation. The temperature-dependent physical properties calculated from the liquid fraction can be expressed as

$$X = \begin{cases} X_i & T < T_{Solidus} \\ (1-\alpha_{Liquid})X_i + \alpha_{Liquid}X_m & T_{Solidus} < T < T_{Liquidus} \\ X_m & T > T_{Liquidus} \end{cases} \tag{22}$$

where X denotes the specific heat (c) or the thermal conductivity (k).

Therefore, the energy equations for all phases in the Solidification/Melting model can be written in a uniform form as

$$\frac{\partial}{\partial t}(\rho h) + \nabla\cdot(\rho \boldsymbol{u} h) = \nabla\cdot(k\nabla T) + S_E \tag{23}$$

where $\boldsymbol{u}$ is the fluid velocity and S_E is the energy source term. With the temperature field solved, the liquid fraction field as well as the freezing front can be obtained.

Besides, the enthalpy-porosity method treats the mushy region (partially solidified region) as a porous medium, whose porosity is equal to the liquid fraction in each cell and decreases from 1 to 0 as the material solidifies. In fully solidified regions, the porosity is equal to zero, which extinguishes the velocities in these regions, and the velocities, therefore, are equal to zero. The reduced porosity (liquid fraction) in the mushy zone will introduce the momentum source term taking the following form,

$$\boldsymbol{S}_M = \frac{(1-\alpha_{Liquid})^2}{\alpha_{Liquid}^3 + \varepsilon}A_{mush}\boldsymbol{u} \tag{24}$$

where ε is a small number (0.001) to prevent division by zero and A_{mush} is the mushy zone constant which measures the damping amplitude of the material velocity. The larger the mush zone constant, the steeper the transition of the material velocity to zero as it solidifies.

The two most important parameters in the Solidification/Melting model is the phase change temperature range $\Delta T_F = T_{Liquidus} - T_{Solidus}$ and the mushy zone constant A_{mush}. Our previous works [60] found that ΔT_F= 0.2 °C is the most suitable value to ensure the interface thickness of the freezing front to be close to the mesh size. This value is eventually chosen as the phase change temperature range for the later simulations. As for the mushy zone constant A_{mush}, the values between 10^4 and 10^7 are recommended for most computations in the Fluent help file [50]. The solidified region may keep an obvious velocity with a very small A_{mush} while a very large A_{mush} may cause the solution to oscillate. The physical meaning of A_{mush} indicates that its value is related to solidification rate which is determined by the supercooling degree ΔT_{SC}, i.e., A_{mush} changes with ΔT_{SC}. Based on the comparisons between the experiments and simulations in the references [38,42,60] and our present work, the variations of the A_{mush} value with the supercooling degree ΔT_{SC} are presented in Table 1.

2.4. Numerical method

Given the assumption that the flow in and around the droplet is axisymmetric, a two-dimensional axisymmetric computational domain is employed, as shown in Fig. 3 (left half). Both the width and height of the rectangle domain are $5D_0$. The bottom surface is regarded as a cold wall with no slip boundary applied. The right and bottom boundaries are the axis and the (cold) wall while the others are set as the pressure outlet boundaries. To better capture the liquid-gas interfaces and improve the computing efficiency, a structured mesh is adopted while a refined grid is applied to the local area where the fluid in the droplet flows.

Table 1
Values for the mushy zone constant A_{mush} at different supercooling degrees [38,42,50,60].

Supercooling degree, ΔT_{SC} (°C)	5	10	15	20	25	30	35
A_{mush}	1.0×10^4	5.0×10^4	1.0×10^5	5.0×10^5	1.0×10^6	5.0×10^6	1.0×10^7

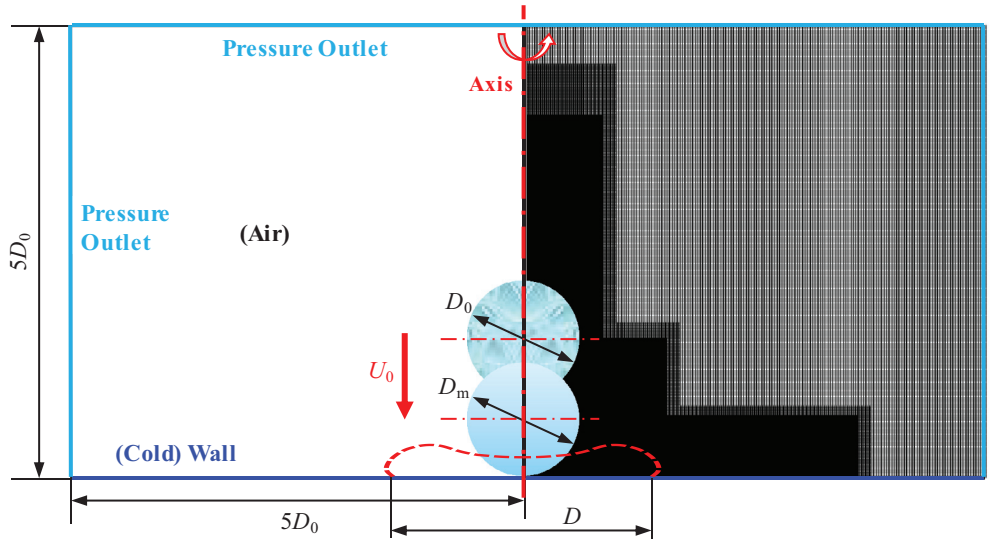

Fig. 3. Physical model (left half) and structured mesh (right half).

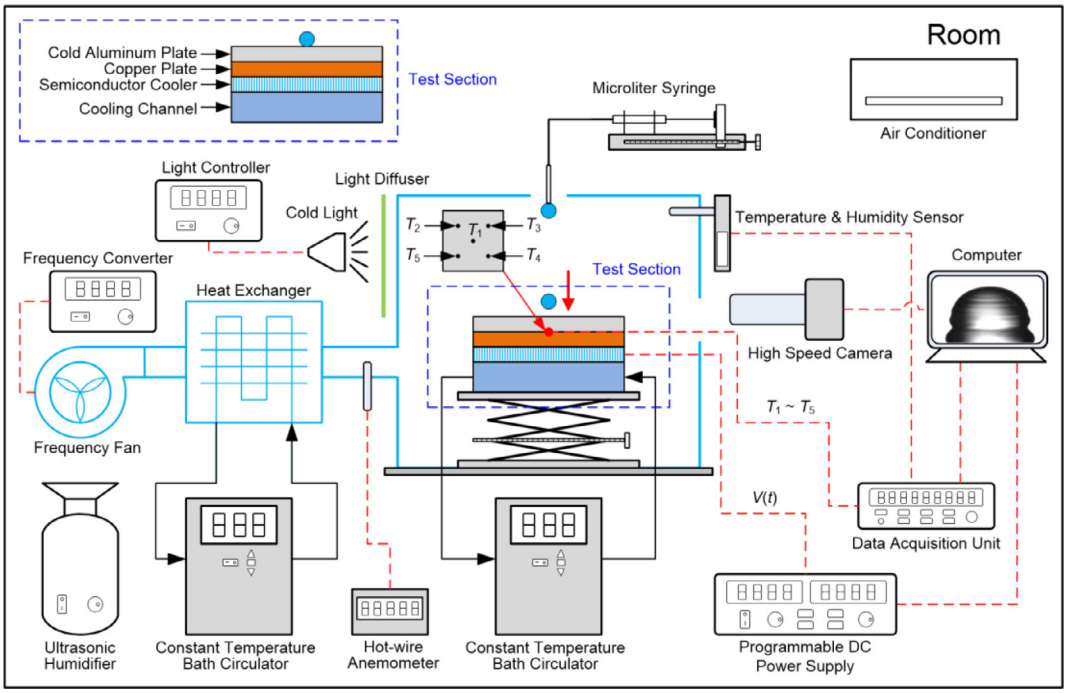

Fig. 4. Schematic diagram of the experimental apparatus.

The commercial CFD software FLUENT v14.5 based on the finite volume method is utilized to solve the conservation equations. The Pressure-Based solver is employed to calculate the transient impacting-freezing process because the fluid can be regarded to be incompressible. The Body Force Weighted [52] and Geo-Reconstruct [50] schemes are used to discretize the pressure and volume fraction. In FLUENT, the Geo-Reconstruct scheme represents the Piecewise-Linear Interface Calculation (PLIC) scheme from the work of Youngs [61] which is the most accurate. The momentum and energy equations are both discretized using the Second Order Upwind method. The PISO (Pressure Implicit Split Operator) scheme is utilized to couple the pressure and velocity. The time discretization uses the First Order Implicit method [50,54,62]. A UDF (User Defined Function) file is embedded to integrate the Kistler DCA model [13,55,56] into the simulation. At the end of each time step, the UDF will automatically calculate the dynamic contact angle using the contact line velocity. This angle will transfer to the next step and act on the liquid-gas interface near the contact line [13].

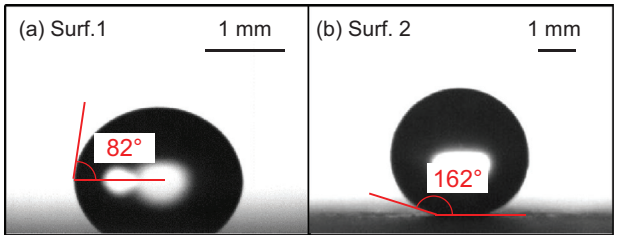

Fig. 5. Contact angles of the experimental surfaces.

3. Experimental work

Fig. 4 illustrates the schematic diagram of the experimental apparatus used in this study, which comprises an environmental control system, a semiconductor thermoelectric cooler system, a data and photograph acquisition system, a droplet generating system and a test section.

The environmental control system is utilized to modulate the air temperature, humidity and velocity in the test section, it consists of an air conditioner, an ultrasonic humidifier, and frequency fan, a heat exchanger, an constant temperature bath and an hot-wire anemometer. By adjusting the frequency fan, the air velocity in the test section is controlled in the range of natural convection ($<0.2 \pm 0.1$ m/s) in our experiments. The room temperature and relative humidity of are 15.0 ± 1 °C and 20±5%. The air temperature in the test section can be cooled down to −5 °C and the corresponding relative humidity is about 60±10%.

The semiconductor cooler system includes a programmable DC power supply (Agilent N5766A, America, 0.02 V regulation accuracy), a semiconductor cooler (TEC1-12706), a channel, and a constant temperature bath. By adjusting the output voltage of the DC power supply, which is connected with the semiconductor cooler, the temperature of the experimental cold plate pasted on the cold side of the cooler is set to the required temperature. A copper plate is sandwiched between the experimental plate and semiconductor cooler to make the plate temperature more uniform, during which high thermal conductive grease is applied to the plate surfaces to reduce the thermal contact resistance. In the experiments, the temperature of the cold surface was set to be −10, −20 and −30 °C with a control accuracy of ±1 °C.

The data and photograph acquisition system consists of five T-type thermocouples (0.127 mm diameter), a temperature and humidity sensor (Rotronic HF532, Switzerland, ±0.1 °C accuracy for temperature and ±0.8% accuracy for humidity), a data acquisition unit (Agilent 34970A, America), a cold light (light diffuser), a high speed camera (Optronis CP80-3-M-540 with a shooting speed of 2000 fps at 1024 pi × 1024 pi resolution and a Nikon AF 105/2.8D

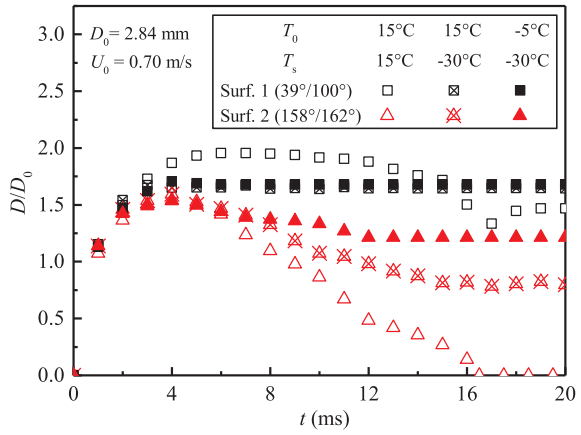

Fig. 7. Evolutions of spreading factors in the impacting-freezing processes of water droplets on hydrophilic Surf. 1 (39°/100°) and superhydrophobic Surf. 2 (158°/162°) under three different sets of experimental droplet (air) and surface temperatures: (I) T_0 = 15 °C, T_s = 15 °C, (II) T_0 = 15 °C, T_s = −30 °C, (III) T_0 = −5 °C, T_s = −30 °C.

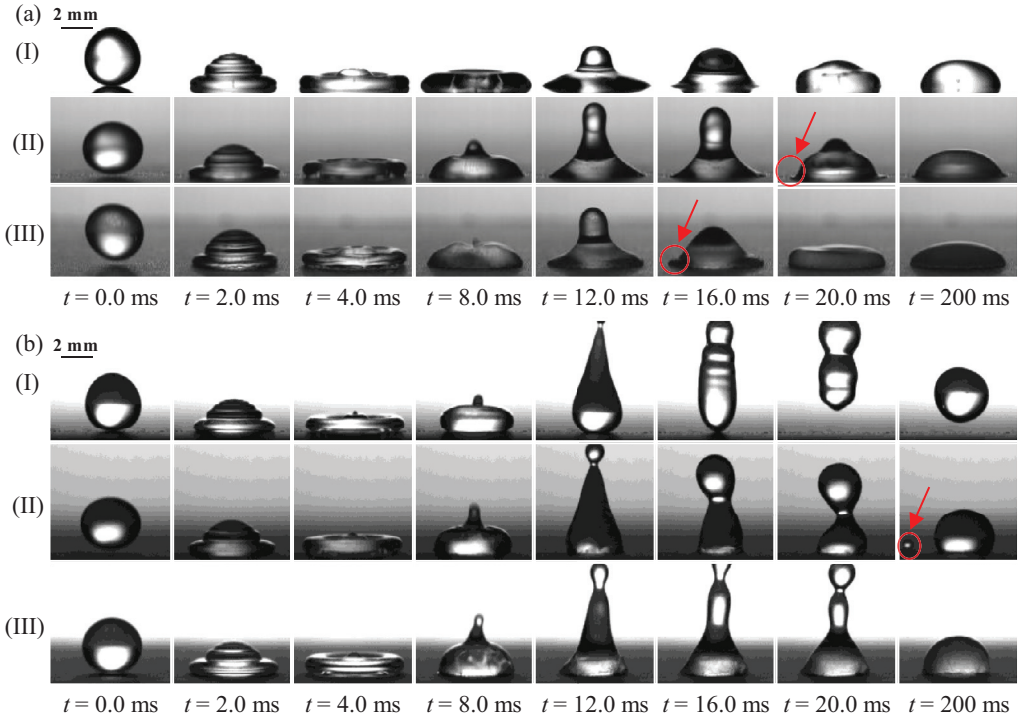

Fig. 6. Impacting-freezing behaviors of water droplets on (a) hydrophilic Surf. 1 (39°/100°) and (b) superhydrophobic Surf. 2 (158°/162°) under three different sets of experimental droplet (air) and surface temperatures: (I) T_0 = 15 °C, T_s = 15 °C, (II) T_0 = 15 °C, T_s = −30 °C, (III) T_0 = −5 °C, T_s = −30 °C.

Table 2
Physical properties of air, water and ice [63].

Material		Density (kg m^{-3})	Heat capacity (kJ kg^{-1} K^{-1})	Thermal conductivity (W m^{-1} K^{-1})	Viscosity (μPa s)	Surface tension (mN m^{-1})	Latent heat (kJ kg^{-1})
Air		1.225	1.005	0.0255	17.894	–	–
Water	15 °C	999.1	4.190	0.589	1153.8	72.74	333.4
	0.1 °C	999.8	4.220	0.561	1791.1	75.65	
	−30 °C	983.8	5.132	0.431	5650.0	79.64	
Ice	−0.1 °C	916.7	2.10	2.16	–	–	
	−30 °C	920.9	1.88	2.50			

Table 3
Maximum and stable spreading factors obtained from the experiments and simulations for different impacting processes.

Spreading factor	Droplet-Surface temperature	Experiment	Simulation	Deviation (%)
Maximum	Room temperature-Room temperature	1.54	1.63	5.84
	Room temperature-Cold [38]	1.60	1.81	11.3
	Supercooled-Cold	1.53	1.63	6.54
Stable	Room temperature-Room temperature	0.00	0.00	0.00
	Room temperature-Cold [38]	1.35	1.25	−7.41
	Supercooled-Cold	1.21	1.19	1.65

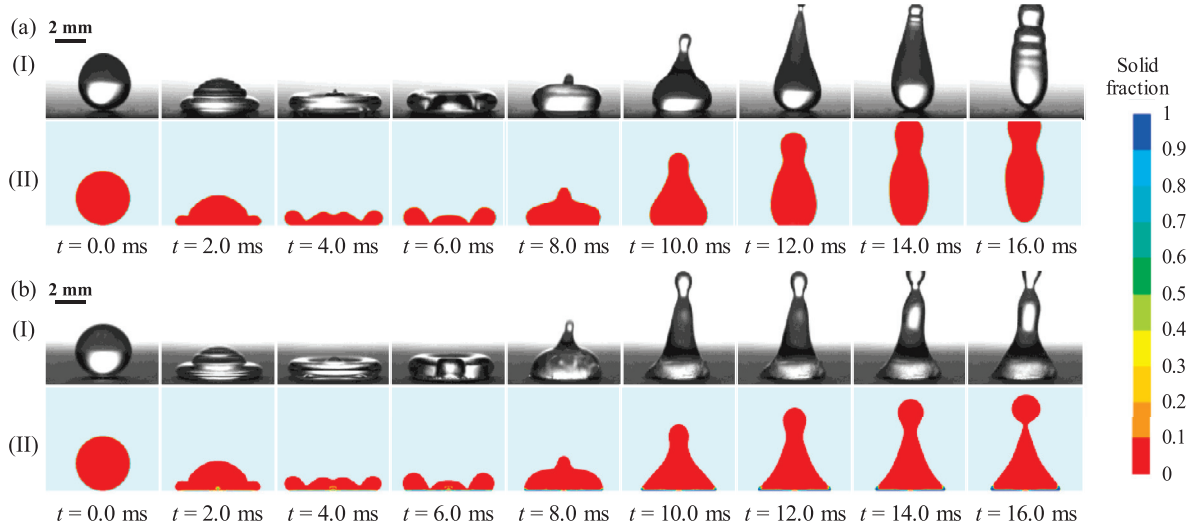

Fig. 8. Comparison of the temporal droplet profiles at different times between (I) experiments and (II) simulations in the impacting processes of (a) a room temperature droplet on the room temperature Surf. 2 (T_0 = 15 °C, T_s = 15 °C) and (b) a supercooled water droplet on the cold Surf. 2 (T_0 = −5 °C, T_s = −30 °C).

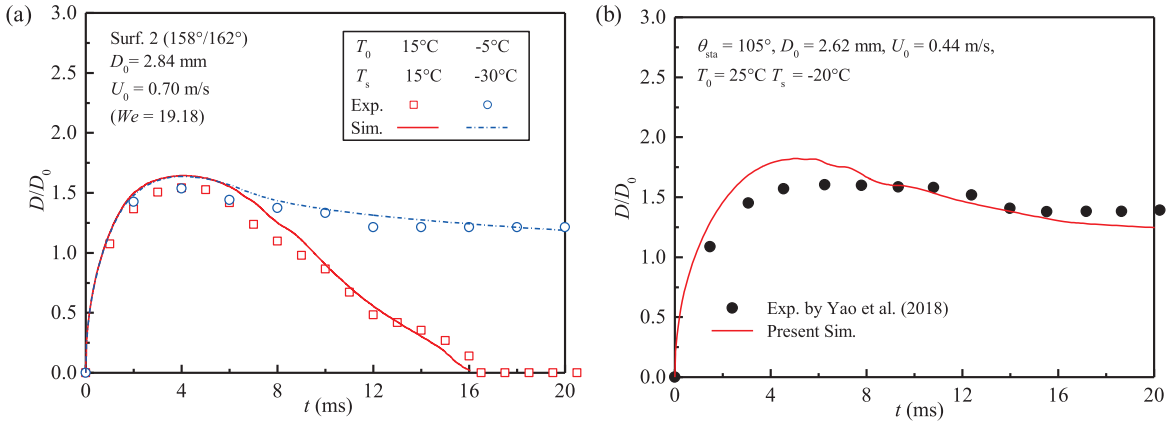

Fig. 9. Comparison of the evolutions of droplet spreading factors obtained from the experiments: (a) experiments and simulations in this work (The impacting processes of a room temperature droplet on the room temperature Surf. 2 and the impacting-freezing process of a supercooled droplet on the cold Surf. 2), (b) experiment in the reference and simulation in this work (The impacting-freezing processes of a room temperature droplet on a cold surface).

Table 4
Simulation conditions.

Droplet volume, V_0 (μL)	Droplet diameter, D_0 (mm)	Weber number, *We*	Static contact angle, θ_{sta} (°)	Supercooling degree, ΔT_{SC} (°C)
5	2.12	10, 30, 50, 70, 90	90	5, 7.5, 10, 12.5, 15
			120	5, 7.5, 10, 12.5, 15, 17.5, 20
			150	5, 7.5, 10, 12.5, 15, 17.5, 20, 22.5, 25, 27.5, 30

lens) and a computer. The computer was used to record the temperature and humidity data and was connected to the high-speed camera for controlling it and storing the acquired images.

The droplet generating system contains a micro-syringe (±0.2 μL accuracy), an adjustable platform and a capillary needle. The outer diameter of the needle used in our experiments is 0.72 mm, yielding an average droplet volume (V_0) of 12 μL and an average droplet diameter (D_0) of 2.84 mm. The droplet initial velocity touching the solid surface (U_0) was calculated to be 0.70 m/s, generating a Weber number of $We = \rho U_0^2 D_0/\sigma =$ 19.18. The temporal droplet profiles were recognized from the experimental data using an image recognition technology in MATLAB R2015b. As a droplet with a diameter of 2.84 mm covers about 250 pi in our experiments, the profile accuracy is about 11.36 μm/pi.

The test section contains an aluminum-based surface (40 mm length × 40 mm width × 1 mm height) inside a closed plexiglass cover (300 mm length × 300 mm width × 300 mm height). By spraying superhydrophobic coating on a bare aluminum surface [14], both hydrophilic (Surf. 1) and superhydrophobic (Surf. 2) surfaces are prepared for the experiments, as shown in Fig. 5. Their static, receding and advancing contact angles are 82°/39°/100° (Surf. 1) and 160°/158°/162° (Surf. 2) measured by a contact angle goniometer (JC2000C1, China, ±1° accuracy).

4. Results and discussion

4.1. Experimental results

Fig. 6 shows the impacting-freezing behaviors of water droplets on the hydrophilic Surf. 1 (39°/100°, Fig. 6a) and superhydrophobic Surf. 2 (158°/162°, Fig. 6b) under three different sets of experimental droplet (air) and surface temperatures: (I) T_0 = 15 °C, T_s = 15 °C, (II) T_0 = 15 °C, T_s = −30 °C and (III) T_0 = −5 °C, T_s = −30 °C. For quantitative comparative analysis, we extract the evolutions of spreading factors during the impacting-freezing processes from the experimental images in Fig. 6 and present them in Fig. 7.

First, we compare the impacting processes of room temperature droplets on room temperature (I) and cold surfaces (II). On the hydrophilic Surf. 1 (39°/100°), the cold surface has little influence on the droplet temporal profiles (Fig. 6a) and spreading factors (Fig. 7) during the early spreading stage (0~3 ms). Near the maximum spreading state (4 ms), the droplet contact line on the cold surface is frozen due to the formation of an ice layer adjacent to the cold Surf. 1. Thus, it stops spreading and the consequent receding stage also disappears while the droplet contact line on a room temperature Surf. 1 experiences the receding stage after the maximum spreading (Fig. 6a). The droplet maximum spreading factor on the cold Surf. 1 is smaller than this on the room temperature one (Fig. 6b) and is equal to its stable spreading factor in our experiment. During the stable stage (after 200 ms), the droplet on the cold Surf. 1 exhibits a smaller stable contact angle and a larger stable spreading factor. On the superhydrophobic Surf. 2 (158°/162°), the cold surface also has little influence on the temporal droplet profiles (Fig. 6b) and spreading factors (Fig. 7) during the entire spreading stage (0~4 ms) and even the early receding

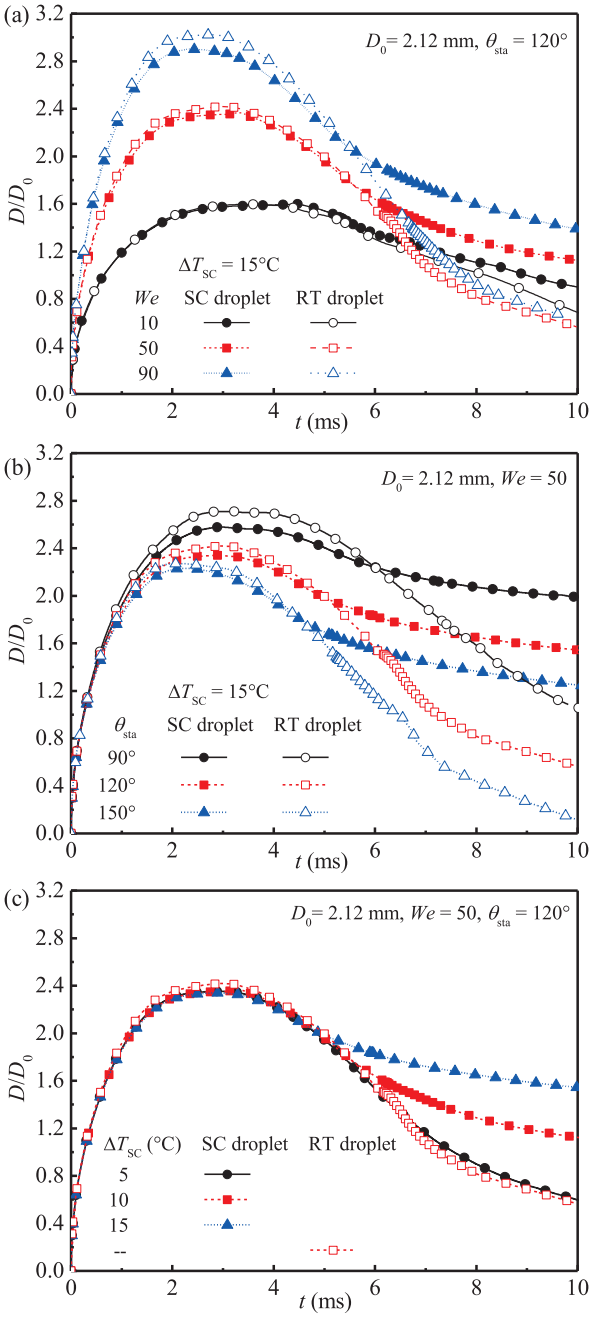

Fig. 10. Effects of (a) Weber number, (b) contact angle and (c) supercooling degree on the evolutions of spreading factors in the impacting-freezing process of a supercooled droplet on a cold surface and in the impacting process of a room temperature droplet on a room temperature surface. SC and RT are the abbreviations for supercooled and room temperature, respectively.

stage (0~4 ms). The high nucleation barrier of superhydrophobic surface [7,21] suppresses the freezing of contact line and delays the start time when the cold surface significantly affects the motion of the contact line as well as the temporal droplet profiles. In Fig. 7, the evolution curves of the spreading factors on room temperature and cold Surf. 2 remain nearly coincident until the early receding stage (6 ms) and the maximum spreading factor remains almost unchanged on the cold Surf. 2. During the receding stage (4~16 ms), the droplet contact line on the cold Surf. 2 shows a much slower retracting velocity than this on a room temperature one, caused by the viscosity increase and the ice layer formation near the cold wall. After the receding stage (200 ms), the satellite droplet (red arrow in Fig. 6b) resulting from the breaking of the droplet upper part adheres to the cold Surf. 2 but bounces off the room temperature one. The anti-icing/frosting and self-cleaning performances of the superhydrophobic surface at the room temperature may disappear for a cold surface. Consequently, the droplet on a cold superhydrophobic surface yields a non-zero stable spreading factor [30,35].

Then, the impacting-freezing processes of room temperature (II) and supercooled (III) water droplets on cold surfaces are also compared. The greatest difference between them is whether the nucleation-recalescence stage exists. This stage is observed after a supercooled water droplet impacts on both the hydrophilic Surf. 1 (39°/100°) and superhydrophobic Surf. 2 (158°/162°). During that stage, the transparency of the supercooled droplet becomes deteriorated and ice crystal grows inside (especially after 8 ms in Fig. 6) as compared to its initial state, which is similar to the previous experimental observations on the freezing process of a sessile supercooled water droplet [18,25]. The supercooled water is changed into the water-ice mixture with the supercooling degree released and the inside temperature returning to the freezing point (0 °C). Thus, the supercooled droplet has a larger viscosity and surface tension during the impacting process than the room temperature droplet, which distinguishes the former impacting-freezing dynamics from the latter. On the hydrophilic Surf. 1 (39°/100°), the supercooled droplet impacting on a cold surface yields a thicker ice layer (red arrow in Fig. 6a) and a smaller droplet height than the room temperature droplet (Fig. 6a) although the evolution curves of their spreading factors almost coincide with each other (Fig. 7). On the superhydrophobic Surf. 2 (158°/162°), the supercooling degree has little influence on the droplet impacting-freezing behaviors until the early receding stage (about 6 ms). After that, the supercooled droplet retracts much more slowly than the room temperature droplet (Fig. 7), yielding a larger stable spreading factor. This induces more concentration of water/ice in the droplet bottom part and the resultant droplet adhesion on the cold Surf. 2.

4.2. Model validation

This work aims to explore the impacting-freezing dynamics of a supercooled water droplet on the cold surface. Owing to the small supercooling degree in the experiments, the numerical method is further used to simulate the impacting-freezing process. Before that, the experimental results in the Section 4.1 is applied to verify the reliability of our numerical model. In our previous work [13], we have validated our model in simulating the two phase flow without freezing. Considering that the following simulations mainly focuses on the impacting-freezing process of a supercooled water droplet on a hydrophobic surface, the experiments in Fig. 6b-(III) is chosen as our simulation conditions while the experiments in Fig. 6b-(I) as the reference. To increase the model reliability, we also simulate the impacting-freezing process of a room temperature water droplet on a hydrophobic surface according to the experimental results in Ref. [38].

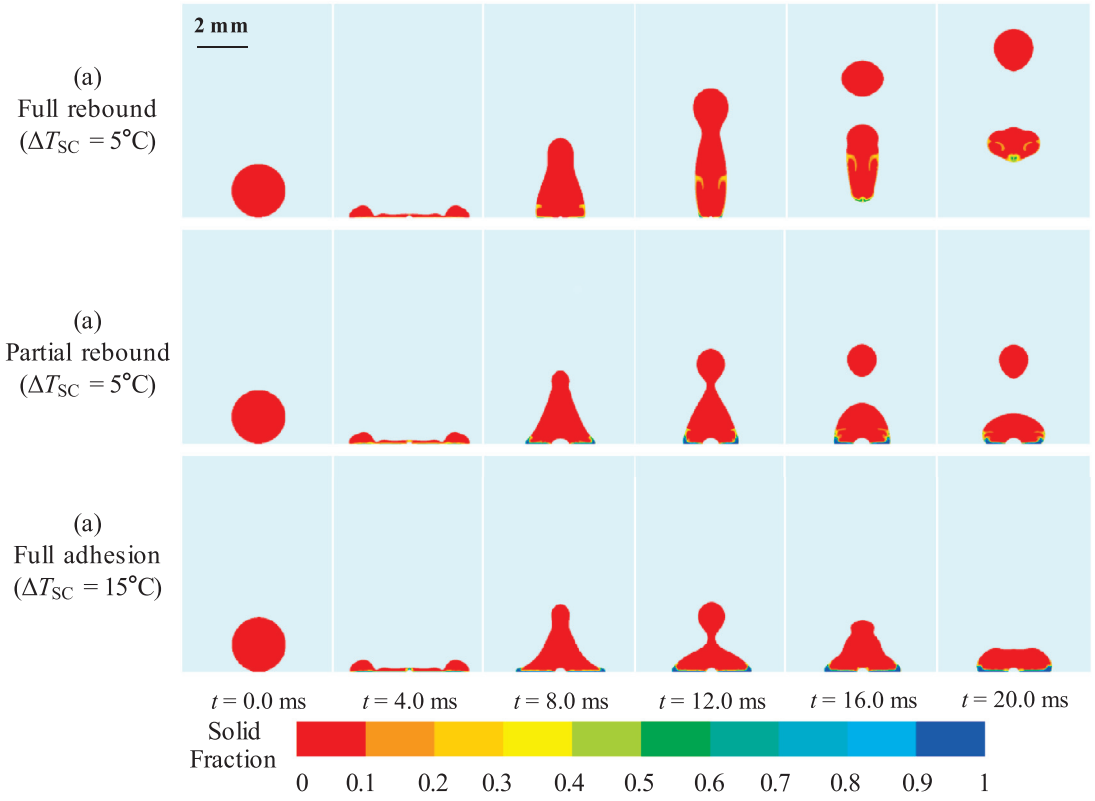

Fig. 11. Three morphologies of (a) full rebound (ΔT_{SC} = 5 °C), (b) partial rebound (ΔT_{SC} = 10 °C) and (c) full adhesion (ΔT_{SC} = 15 °C) when a supercooled water droplet impacts on cold hydrophobic surfaces (θ_{sta} = 120°, *We* = 50) having different supercooling degrees.

The physical properties of air, water and ice used in the simulations are presented in Table 2 [63]. A variable time step is utilized by controlling the Courant number under 0.1 while the maximum time step is controlled to 10^{-6} s. All the residuals are set to be 10^{-6} s. Thus, the real time step in the simulation varies within the range of 10^{-9} ~ 10^{-6} s. To test the mesh independence, four different square grids having sizes of 40 μm × 40 μm, 20 μm × 20 μm, 10 μm × 10 μm and 5 μm × 5 μm are tested in the simulation. The difference between the maximum spreading factors yielded by 10 μm × 10 μm and 5 μm × 5 μm meshes is less than 1%. With a compromise made between the computation time and accuracy, the mesh size used in the following simulation is eventually chosen as 10 μm × 10 μm.

Fig. 8 shows the droplet temporal profiles at different times during the impacting processes of a room temperature droplet on the room temperature Surf. 2 (T_0 = 15 °C, T_s = 15 °C) and a supercooled water droplet on the cold Surf. 2 (T_0 = −5 °C, T_s = −30 °C), observed in the experiments and simulations. Regardless of the freezing in the droplet impacting process, the calculated temporal droplet profiles agree well with the experimental observations. Fig. 9 further illustrates the quantitative comparisons of the spreading factors obtained from the experiments and simulations. The maximum and stable spreading factors yielded by the experiments and simulations for different impacting and freezing processes are listed in Table 3. The maximum deviation of the maximum and stable spreading factors between experiments and simulations is 11.3% which is mainly caused by the lack of accurate advancing and receding contact angles in Fig. 9b. Considering the complex fluid flow and phase change in the impacting-freezing process of a supercooled drop and the empirical mushy parameter A_{mush}, this deviation is acceptable. All the above comparisons support the reliability of our simulation model and demonstrate that this model can be used for the simulation and analysis of impacting-freezing process of a supercooled or room temperature droplet on a cold surface.

4.3. Effects of Weber number, contact angle and supercooling degree on the spreading factor

It is possible for a room temperature droplet to bounce off the room temperature surface in the impacting process only when the surface is hydrophobic [15], i.e., $\theta_{sta} > 90°$. In this work, we focus on the surface anti-icing performances and thus mainly investigate the impacting-freezing process of a supercooled water droplet on the hydrophobic cold surface. Calculations are made for a series of conditions as presented in Table 4. The Weber number varies over 10 ~ 90, ensuring that the contact line stability is not destroyed and the droplet is axisymmetric in the impacting process. The static contact angle of the hydrophobic surface is 90°, 120° and 150°. The present work aims to explore the effect of the static contact angle of a smooth surface on the impacting-freezing dynamics, and a representative contact angle hysteresis for a smooth surface based on our previous experiments [14] is approximately 20°. For convenience, this value is set to be the contact angle hysteresis in the DCA model. The static contact angle is taken as the average of the advancing and receding contact angles. Thus, $\theta_{adv} = \theta_{sta} + 10°$ and $\theta_{rec} = \theta_{sta} - 10°$. It should be noticed that θ_{adv} and θ_{rec} are used in Eq. (13) to determine the equilibrium contact angle θ_{eq} while the dynamic contact angle θ_d in the impacting-freezing process is calculated by the Kistler's DCA model. The supercooling degree range is 5 ~ 30 °C. In most practical applications, the supercooled water droplet and the cold surface are usually exposed to the same environment. Hence, they have the same supercooling degree in the following simulations.

Fig. 10 indicates the effects of the contact angle and supercooling degree on the spreading factors in the impacting-freezing process of a supercooled droplet on a cold surface, with the impacting process of a room temperature droplet on a room temperature surface as the reference. As the Weber number goes up and the contact angle decreases (Fig. 10a-b), the supercooled droplet spreads faster as the room temperature droplet does [12,13], generating a larger maximum spreading factor. The supercooling degree has little influence on the droplet spreading as well as the maximum spreading factor (Fig. 10c). Similar to the experimental results in Figs. 5 and 6, the supercooled water droplet spreads and retracts slower than the room temperature one on the cold surface and thus yields a smaller maximum spreading factor and larger stable one. These differences become more conspicuous with the increases of the Weber number and supercooling degree and the decrease of the contact angle. A bigger Weber number and a less

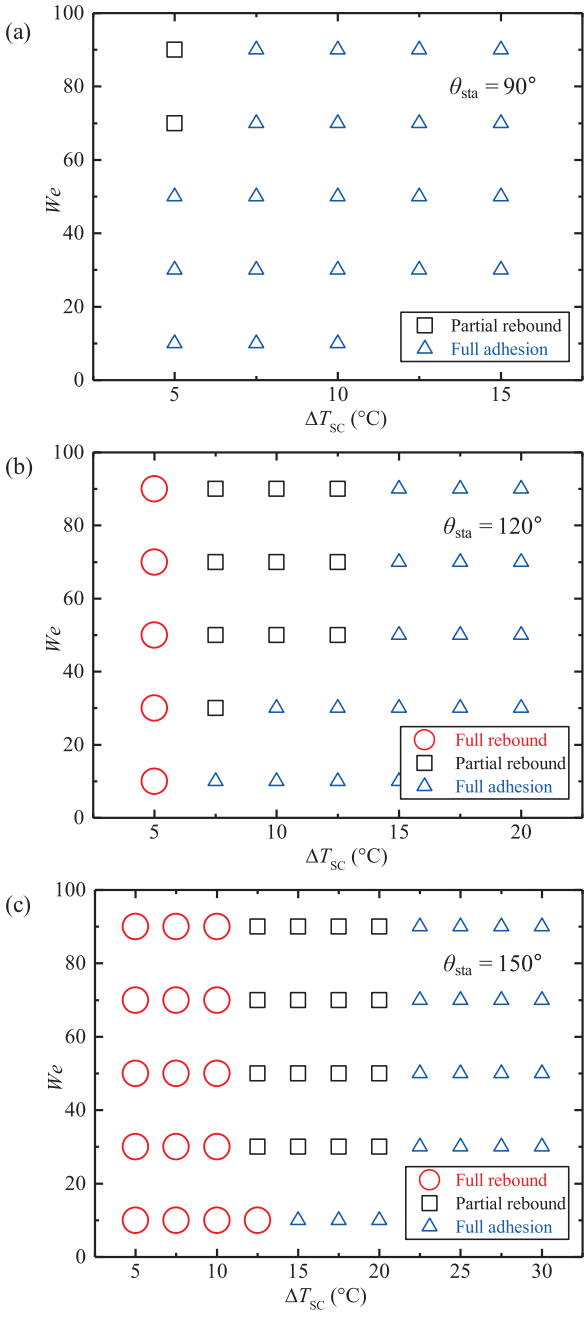

Fig. 12. Morphology map of the rebound and adhesion when a supercooled water droplet impacts on a cold hydrophobic surface under different Weber numbers, supercooling degrees and contact angles.

hydrophobic surface both enlarge the spreading factor, enhancing the heat transfer between the supercooled droplet and the cold surface. A greater supercooling degree lowers the latent heat of the water-ice mixture after the nucleation-recalescence stage and enlarges the phase change driving force. These accelerate the formation of the ice layer near the cold surface which causes the differences between the impacting-freezing process of a supercooled droplet and the impacting process of a room temperature droplet. In Fig. 10, the contact line shows a very slow receding velocity even after it is solidified but it remains completely pinned in the experiment. This is due to the limitation of the Solidification/Melting model. In the physical process, the contact line will certainly be pinned after it is completely solidified, which indicates that the momentum source term approaches infinity. However, in the simulation, the larger momentum source $\boldsymbol{S}_M$ as shown by Eq. (24) will induce a great velocity gradient and may cause the solution to oscillate or diverge. So, ε needs to be set as a small number (e.g., 0.001) and A_{mush} is recommended to take a finite value in the momentum source term of Eq. (24), which ensures the finite $\boldsymbol{S}_M$ value and the simulation convergence even in the fully solidified region ($\alpha_{Liquid}= 0$).

4.4. Morphology of rebound and adhesion

After a supercooled water droplet impacts on a cold surface at the same Weber number, it will exhibit three different morphologies at different supercooling degrees as shown in Fig. 11, namely full rebound, partial rebound and full adhesion, indicating a competition between the fluid flow (reflected by the Weber number) and heat transfer (or phase change, characterized by the supercooling degree) near the cold surface. The above three morphologies are also observed in the impacting-freezing process of a room temperature droplet on a cold hydrophobic surface [30,35]. At a smaller supercooling degree (Fig. 11a), the contact line motion in the impacting-freezing process is dominated by the fluid flow inside the droplet while little liquid is frozen near the cold surface due to the weak heat transfer and slow freezing speed. The droplet finally bounces off the cold surface. On the contrary, a larger supercooling degree (Fig. 11c) enhances the heat transfer and increases the liquid freezing speed. Consequently, the contact line is frozen in the impacting-freezing process and the droplet finally adheres to the cold surface. At an intermediate supercooling degree (Fig. 11b), the upper part breaks away from the droplet while the bottom part sticks to the cold surface. The above competitive relationship between the impacting and freezing process reveals that the anti-icing of a hydrophobic surface is related to the supercooling degree of the environment.

Based on the definitions of three droplet morphologies (Fig. 11), Fig. 12 illustrates the morphology map of the rebound and adhesion when a supercooled water droplet impacts on a cold hydrophobic surface having the same supercooling degree under different Weber numbers, supercooling degrees and contact angles. When the surface becomes more hydrophobic, the limits for the full rebound and adhesion both shift to the larger supercooling degree. A more hydrophobic surface results in a smaller spreading factor [12,13], weakening the heat transfer and the liquid freezing. Thus, the droplet is easier to bounce off the cold surface at the same Weber number and supercooling degree. That is to say, a greater supercooling degree is needed for the full adhesion of a supercooled droplet on a more hydrophobic surface. It is noticed that the droplet shows either full rebound or full adhesion while partial rebound is not observed at a low Weber number (We = 10) in Fig. 12. This is because the inertial force is too weak to break the droplet in the impacting-freezing process compared to the surface tension.

In the impacting-freezing process of a supercooled water droplet, the heat transfer between the droplet and cold surface is related to the contact area except for the supercooling degree. This area can be calculated from the spreading factor. The energy analysis of the impacting process suggests that the maximum spreading

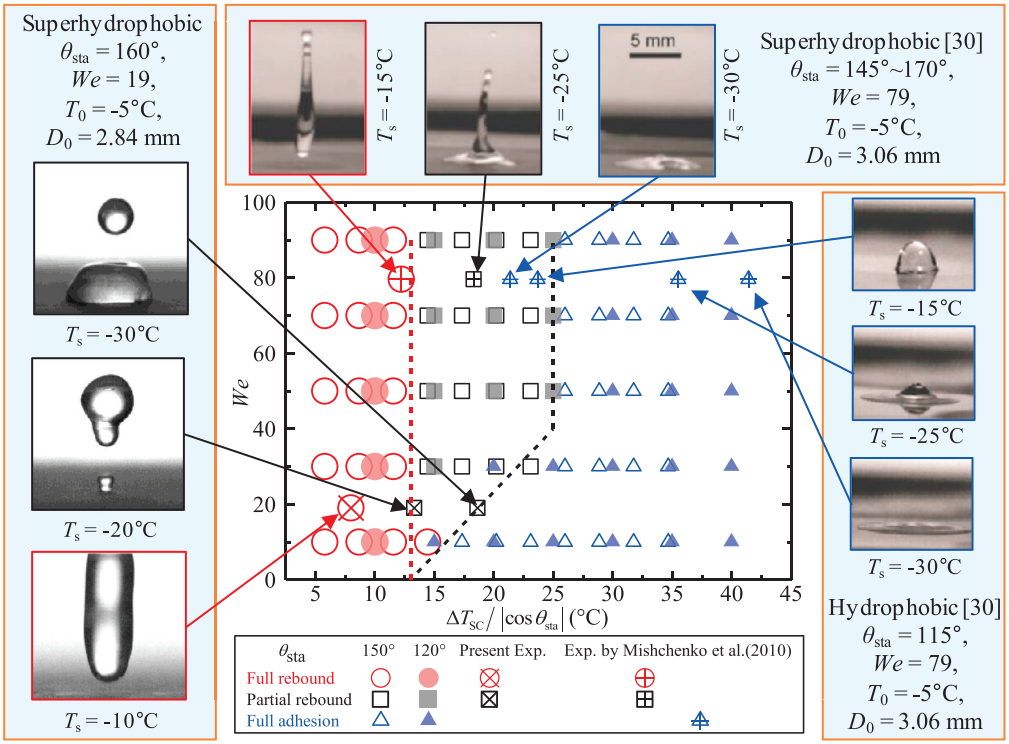

Fig. 13. Unified morphology map of the rebound and adhesion when a supercooled water droplet impacts on cold hydrophobic surface under different Weber numbers, supercooling degrees and contact angles.

factor can be expressed as [13,15],

$$\left(\frac{D_{\max}}{D_0}\right)^2 = \frac{We+12}{3(1-\cos\theta_{sta})+\frac{4We}{\sqrt{Re}}} \tag{25}$$

This equation indicates that the morphology of the rebound and adhesion is determined by a function of $f(We, \Delta T_{SC}, \cos\theta_{sta})$. The limits for the full rebound and full adhesion can thus be written as

$$We \sim f(\Delta T_{SC},\ \cos\theta_{sta}) \tag{26}$$

Fig. 12 further shows that the increase of the contact angle θ_{sta} will enlarge the limits of supercooling degree for the full rebound and full adhesion while $\Delta T_{SC}/|\cos\theta_{sta}|$ near the limits remains almost constant for different hydrophobic surfaces ($90^\circ < \theta_{sta} < 180^\circ$). Replacing the abscissa ΔT_{SC} in Fig. 12 with $\Delta T_{SC}/|\cos\theta_{sta}|$, the unified morphology map of the rebound and adhesion when a supercooled water droplet impacts on a cold surface under different Weber numbers, contact angles and supercooling degrees are obtained and presented in Fig. 13. Most points in present experimental observations and in Ref. [30] both agree well with the morphologies map. Here, the reference supercooling degree is taken as the average of the supercooled water droplet and the cold surface if they have different supercooling degrees. The figure clarifies the quantitative competitive relationship between the fluid flow and phase change in the impacting-freezing process of a supercooled water droplet. Importantly, Fig. 13 also provides the universal limits for the full rebound and adhesion, i.e.,

$$\text{Full rebound}: \frac{\Delta T_{SC}}{|\cos\theta_{sta}|} \lesssim 13,\ 0 < We \lesssim 90 \tag{27}$$

$$\text{Full adhesion}: \begin{cases} \frac{\Delta T_{SC}}{|\cos\theta_{sta}|} \gtrsim 25,\ 40 \lesssim We \lesssim 90 \\ \frac{10}{3}\left(\frac{\Delta T_{SC}}{|\cos\theta_{sta}|}-13\right)+We \lesssim 0,\ 0 < We \lesssim 40 \end{cases} \tag{28}$$

They are the concrete formulas of Eq. (26).

5. Conclusions

Simulations and experiments are conducted to study the impacting-freezing dynamics of a supercooled water droplet on a cold surface, with the impacting dynamics of a room temperature droplet on a room temperature surface being included in the comparison. The influences of the Weber number, contact angle and supercooling degree on the spreading factor and the droplet morphology of rebound and adhesion are investigated. The following conclusions are drawn:

(1) The numerical model considering the supercooling effect in the initial conditions can be used to simulate the impacting-freezing behaviors of a supercooled water droplet on the cold surface. Both the temporal droplet profile and the spreading factor yielded by the simulations agree well with the experimental observations. The maximum deviation of the maximum and stable spreading factors between experiments and simulations is 11.3%.

(2) The supercooled droplet spreads and retracts slower than the room temperature one in the impacting process and thus yields a smaller maximum spreading factor and a larger stable spreading factor. These differences become more conspicuous with the increases of the Weber number and supercooling degree and the decrease of the contact angle.

(3) The supercooled droplet impacting on a clod hydrophobic surface exhibits three different morphologies of full rebound, partial rebound and full adhesion, which indicates a competition between the fluid flow and heat transfer (phase change) in the impacting-freezing process. A unified morphology map of rebound and adhesion correlating the Weber number, supercooling degree and contact angle for the impacting-freezing behavior is obtained and it provides the universal limits for the full rebound and adhesion.

Declaration of Competing Interest

The authors declare that they have no known competing financial interests or personal relationships that could have appeared to influence the work reported in this paper.

CRediT authorship contribution statement

Xuan Zhang: Conceptualization, Methodology, Software, Validation, Formal analysis, Investigation, Writing - original draft. **Xin Liu:** Software, Methodology, Validation, Investigation. **Xiaomin Wu:** Supervision, Writing - review & editing. **Jingchun Min:** Supervision, Writing - review & editing, Funding acquisition.

Acknowledgements

This research is funded by the National Key Basic Research Program of China (No. 2015CB755800) and the International Postdoctoral Exchange Fellowship Program (No. 20190005).

Supplementary materials

Supplementary material associated with this article can be found, in the online version, at doi:10.1016/j.ijheatmasstransfer.2020.119997.

References

[1] Y. Cao, Z. Wu, Y. Su, Z. Xu, Aircraft flight characteristics in icing conditions, Prog. Aerosp. Sci. 74 (2015) 62–80.
[2] X. Zhang, X.M. Wu, J.C. Min, Aircraft icing model considering both rime ice property variability and runback water effect, Int. J. Heat Mass Transf. 104 (2017) 510–516.
[3] N. Dalili, A. Edrisy, R. Carriveau, A review of surface engineering issues critical to wind turbine performance, Renew. Sustain. Energy Rev. 13 (2) (2009) 428–438.
[4] H.J. Punge, M. Kunz, Hail observations and hailstorm characteristics in Europe: a review, Atmos. Res. 176–177 (2016) 159–184.
[5] X.M. Wu, R.L. Webb, Investigation of the possibility of frost release from a cold surface, Exp. Therm. Fluid Sci. 24 (3–4) (2001) 151–156.
[6] M.A. Rahman, A.M. Jacobi, Experimental study on frosting/defrosting characteristics of microgrooved metal surfaces, Int. J. Refrig. 50 (2015) 44–56.
[7] F. Chu, X.M. Wu, L. Wang, Dynamic melting of freezing droplets on ultraslippery superhydrophobic surfaces, ACS Appl. Mater. Inter. 9 (9) (2017) 8420–8425.
[8] X. Wu, V.V. Silberschmidt, Z. Hu, Z. Chen, When superhydrophobic coatings are icephobic: role of surface topology, Surf. Coat. Technol. 358 (2019) 207–214.
[9] C. Wang, H. Tsai, Y. Wu, W. Hwang, Investigation of molten metal droplet deposition and solidification for 3d printing techniques, J. Micromech. Microeng. 26 (9) (2016) 95012.
[10] C. Le Bot, S. Vincent, E. Arquis, Impact and solidification of indium droplets on a cold substrate, Int. J. Therm. Sci. 44 (3) (2005) 219–233.
[11] A.L. Yarin, Drop impact dynamics: splashing, spreading, receding, bouncing..., Annu. Rev. Fluid Mech. 38 (1) (2006) 159–192.
[12] Š. Šikalo, M. Marengo, C. Tropea, E.N. Ganić, Analysis of impact of droplets on horizontal surfaces, Exp. Therm. Fluid Sci. 25 (7) (2002) 503–510.
[13] X. Liu, X. Zhang, J.C. Min, Maximum spreading of droplets impacting spherical surfaces, Phys. Fluids 31 (9) (2019) 92102.
[14] X. Liu, X. Zhang, J.C. Min, Spreading of droplets impacting different wettable surfaces at a weber number close to zero, Chem. Eng. Sci. 207 (2019) 495–503.
[15] T. Mao, D.C.S. Kuhn, H. Tran, Spread and rebound of liquid droplets upon impact on flat surfaces, AIChe J. 43 (9) (1997) 2169–2179.
[16] Y. Liu, L. Moevius, X. Xu, T. Qian, J.M. Yeomans, Z. Wang, Pancake bouncing on superhydrophobic surfaces, Nat. Phys. 10 (7) (2014) 515–519.
[17] A. Alizadeh, M. Yamada, R. Li, W. Shang, S. Otta, S. Zhong, L. Ge, A. Dhinojwala, K.R. Conway, V. Bahadur, A.J. Vinciquerra, B. Stephens, M.L. Blohm, Dynamics of ice nucleation on water repellent surfaces, Langmuir 28 (6) (2012) 3180–3186.
[18] X. Zhang, X.M. Wu, J.C. Min, Freezing and melting of a sessile water droplet on a horizontal cold plate, Exp. Therm. Fluid Sci. 88 (2017) 1–7.

[19] Z. Meng, P. Zhang, Dynamic propagation of ice-water phase front in a supercooled water droplet, Int. J. Heat Mass Transf. 152 (2020) 119468.
[20] X. Zhang, X. Liu, X.M. Wu, J.C. Min, Experimental investigation and statistical analysis of icing nucleation characteristics of sessile water droplets, Exp. Therm. Fluid Sci. 99 (2018) 26–34.
[21] P. Hao, C. Lv, X. Zhang, Freezing of sessile water droplets on surfaces with various roughness and wettability, Appl. Phys. Lett. 104 (16) (2014) 161609.
[22] C. Marcolli, Ice nucleation triggered by negative pressure, Sci. Rep. 7 (1) (2017) 16634.
[23] R.R. Czys, Ice initiation by collision-freezing in warm-based cumuli, J. Appl. Meteorol. 28 (10) (1989) 1098–1104.
[24] X. Zhang, X.M. Wu, J.C. Min, X. Liu, Modelling of sessile water droplet shape evolution during freezing with consideration of supercooling effect, Appl. Therm. Eng. 125 (2017) 644–651.
[25] S. Jung, M.K. Tiwari, N.V. Doan, D. Poulikakos, Mechanism of supercooled droplet freezing on surfaces, Nat. Commun. 3 (1) (2012) 615.
[26] Á.G. Marín, O.R. Enríquez, P. Brunet, P. Colinet, J.H. Snoeijer, Universality of tip singularity formation in freezing water drops, Phys. Rev. Lett. 113 (5) (2014) 54301.
[27] X. Zhang, X. Liu, J.C. Min, X.M. Wu, Shape variation and unique tip formation of a sessile water droplet during freezing, Appl. Therm. Eng. 147 (2019) 927–934.
[28] H. Zhang, Y. Zhao, R. Lv, C. Yang, Freezing of sessile water droplet for various contact angles, Int. J. Therm. Sci. 101 (2016) 59–67.
[29] T.V. Vu, G. Tryggvason, S. Homma, J.C. Wells, Numerical investigations of drop solidification on a cold plate in the presence of volume change, Int. J. Multiphas. Flow 76 (2015) 73–85.
[30] L. Mishchenko, B. Hatton, V. Bahadur, J.A. Taylor, T. Krupenkin, J. Aizenberg, Design of ice-free nanostructured surfaces based on repulsion of impacting water droplets, ACS Nano 4 (12) (2010) 7699–7707.
[31] Z. Jin, H. Zhang, Z. Yang, The impact and freezing processes of a water droplet on different cold cylindrical surfaces, Int. J. Heat Mass Transf. 113 (2017) 318–323.
[32] J. Ju, Z. Jin, H. Zhang, Z. Yang, J. Zhang, The impact and freezing processes of a water droplet on different cold spherical surfaces, Exp. Therm. Fluid Sci. 96 (2018) 430–440.
[33] Z. Jin, H. Zhang, Z. Yang, Experimental investigation of the impact and freezing processes of a water droplet on an ice surface, Int. J. Heat Mass Transf. 109 (2017) 716–724.
[34] M. Schremb, I.V. Roisman, C. Tropea, Transient effects in ice nucleation of a water drop impacting onto a cold substrate, Phys. Rev. E 95 (2) (2017) 22805.
[35] B. Ding, H. Wang, X. Zhu, R. Chen, Q. Liao, Water droplet impact on superhydrophobic surfaces with various inclinations and supercooling degrees, Int. J. Heat Mass Transf. 138 (2019) 844–851.
[36] Y. Chen, Y. Fu, J. Huang, Z. Luo, D. Mo, S. Lyu, Droplet bouncing on hierarchical branched nanotube arrays above and below the freezing temperature, Appl. Surf. Sci. 375 (2016) 127–135.
[37] T. Maitra, M.K. Tiwari, C. Antonini, P. Schoch, S. Jung, P. Eberle, D. Poulikakos, On the nanoengineering of superhydrophobic and impalement resistant surface textures below the freezing temperature, Nano Lett. 14 (1) (2013) 172–182.
[38] Y. Yao, C. Li, Z. Tao, R. Yang, H. Zhang, Experimental and numerical study on the impact and freezing process of a water droplet on a cold surface, Appl. Therm. Eng. 137 (2018) 83–92.
[39] R. Zhang, P. Hao, X. Zhang, F. He, Supercooled water droplet impact on superhydrophobic surfaces with various roughness and temperature, Int. J. Heat Mass Transf. 122 (2018) 395–402.
[40] M. Sun, W. Kong, F. Wang, H. Liu, Impact freezing modes of supercooled droplets determined by both nucleation and icing evolution, Int. J. Heat Mass Transf. 142 (2019) 118431.
[41] L. Wang, W. Kong, F. Wang, H. Liu, Effect of nucleation time on freezing morphology and type of a water droplet impacting onto cold substrate, Int. J. Heat Mass Transf. 130 (2019) 831–842.
[42] J. Blake, D. Thompson, D. Raps, T. Strobl, Simulating the freezing of supercooled water droplets impacting a cooled substrate, AIAA J. 53 (7) (2015) 1725–1739.
[43] Y. Yao, C. Li, H. Zhang, R. Yang, Modelling the impact, spreading and freezing of a water droplet on horizontal and inclined superhydrophobic cooled surfaces, Appl. Surf. Sci. 419 (2017) 52–62.
[44] S. Chang, L. Ding, M. Song, M. Leng, Numerical investigation on impingement dynamics and freezing performance of micrometer-sized water droplet on dry flat surface in supercooled environment, Int. J. Multiphas. Flow 118 (2019) 150–164.
[45] M. Tembely, R. Attarzadeh, A. Dolatabadi, On the numerical modeling of supercooled micro-droplet impact and freezing on superhydrophobic surfaces, Int. J. Heat Mass Transf. 127 (2018) 193–202.
[46] M. Schremb, I.V. Roisman, C. Tropea, Normal impact of supercooled water drops onto a smooth ice surface: experiments and modelling, J. Fluid Mech 835 (2018) 1087–1107.
[47] R. de Ruiter, P. Colinet, P. Brunet, J.H. Snoeijer, H. Gelderblom, Contact line arrest in solidifying spreading drops, Phys. Rev. Fluids 2 (4) (2017) 43602.
[48] O.R. Enríquez, Á.G. Marín, K.G. Winkels, J.H. Snoeijer, Freezing singularities in water drops, Phys. Fluids 24 (9) (2012) 91102.
[49] C.W. Hirt, B.D. Nichols, Volume of fluid (VOF) method for the dynamics of free boundaries, J. Comput. Phys. 39 (1) (1981) 201–225.
[50] , ANSYS FLUENT User Guide, Release 14.5, ANSYS Inc., Canonsburg, PA, USA, 2012 October.
[51] Š. Šikalo, H.D. Wilhelm, I.V. Roisman, S. Jakirlić, C. Tropea, Dynamic contact angle of spreading droplets: experiments and simulations, Phys. Fluids 17 (6) (2005) 62103.
[52] B. Ji, Q. Song, Q. Yao, Numerical study of hydrophobic micron particle's impaction on liquid surface, Phys. Fluids 29 (7) (2017) 77102.
[53] K. Yokoi, D. Vadillo, J. Hinch, I. Hutchings, Numerical studies of the influence of the dynamic contact angle on a droplet impacting on a dry surface, Phys. Fluids 21 (7) (2009) 72102.
[54] I. Malgarinos, N. Nikolopoulos, M. Marengo, C. Antonini, M. Gavaises, VOF simulations of the contact angle dynamics during the drop spreading: standard models and a new wetting force model, Adv. Colloid Interface Sci. 212 (2014) 1–20.
[55] H.B. Eral, D.J.C.M.T Mannetje, J.M. Oh, Contact angle hysteresis: a review of fundamentals and applications, Colloid Polym. Sci. 291 (2) (2013) 247–260.
[56] T. Jiang, O.H. Soo-Gun, J.C. Slattery, Correlation for dynamic contact angle, J. Colloid Interface Sci. 69 (1) (1979) 74–77.
[57] O.V. Voinov, Hydrodynamics of wetting, Fluid Dyn. 11 (5) (1977) 714–721.
[58] F. Feuillebois, A. Lasek, P. Creismeas, F. Pigeonneau, A. Szaniawski, Freezing of a subcooled liquid droplet, J. Colloid Interface Sci. 169 (1) (1995) 90–102.
[59] A. Bejan, A.D. Kraus, Heat Transfer Handbook, John Wiley & Sons, Hoboken, New Jersey, 2003.
[60] X. Zhang, X. Liu, X.M. Wu, J.C. Min, Simulation and experiment on supercooled sessile water droplet freezing with special attention to supercooling and volume expansion effects, Int. J. Heat Mass Transf. 127 (A) (2018) 975–985.
[61] D.L. Youngs, Time-dependent multi-material flow with large fluid distortion, in: K.W. Morton, M.J. Baines (Eds.), Numerical Methods for Fluid Dynamics, Academic Press, New York, NY, USA, 1982, pp. 273–486.
[62] H. Huang, X. Chen, Energetic analysis of drop's maximum spreading on solid surface with low impact speed, Phys. Fluids 30 (2) (2018) 22106.
[63] W.M. Haynes, CRC Handbook of Chemistry and Physics, 95th ed., CRC Press, Boca Raton, Florida, 2014.